Three-Phase *LLC* Battery Charger: Wide Regulation and Improved Light-Load Operation

Sayed Abbas Arshadi, *Student Member, IEEE*, Martin Ordonez, *Member, IEEE*, Wilson Eberle, *Member, IEEE*, Marian Craciun, *Member, IEEE*, and Chris Botting, *Member, IEEE*

***Abstract*—Three-phase *LLC* resonant converters can handle much higher power compared to half-bridge and full-bridge *LLC* converters, which makes them suitable for levels 2 and 3 battery charger applications. In addition to the unique features of *LLC* resonant converters, the three-phase structure provides higher power capacity and higher power density at higher power levels in comparison with single-phase structures. Although single-phase *LLC* resonant converters were thoroughly investigated in the literature for many different applications, limited work has been done on three-phase *LLC* converters. Unexplored problems with three-phase *LLC* resonant converters include issues with their limited gain range and also their poor light-load efficiency. In this article, a modified three-phase *LLC* resonant converter with a new phase-shedding strategy is proposed. With the proposed modified topology and phase-shedding strategy, the wide gain range needed for covering the recovery zone of charging Li-ion batteries is realized. Moreover, with the proposed phase-shedding strategy, a significant efficiency improvement with light-load absorption charging is achieved. A 3-kW prototype was developed to validate the performance of the proposed converter.**

***Index Terms*—Battery charger, dead battery, extended gain range, light-load, phase-shedding, recovery charging, three-phase *LLC*.**

I. Introduction

OVER the past decade, the use of battery-powered equipment such as electric vehicle (EV), laptops, and cellphones has increased drastically. This has led to a significant market increase in the batteries sector and greater interest in improving the performance. Battery chargers are the power processing stage between energy sources and batteries. In order to be able to cope with newer technological requirements, higher efficiency, higher power density, and enhanced reliability are expected from this type of power converter. The safety, durability, and performance of batteries are highly dependent on how they are charged and discharged [1].

Manuscript received January 23, 2020; revised April 16, 2020; accepted June 25, 2020. Date of publication July 1, 2020; date of current version September 22, 2020. This work was supported by the Natural Sciences and Engineering Research Council, Canada. Recommended for publication by Associate Editor R.-L. Lin. *(Corresponding author: Sayed Abbas Arshadi.)*

Sayed Abbas Arshadi, Martin Ordonez, and Wilson Eberle are with the Department of Electrical and Computer Engineering, The University of British Columbia, Vancouver, BC V6T 1Z4, Canada (e-mail: arshadi@ieee.org; mordonez@ieee.org; wilson.eberle@ubc.ca).

Marian Craciun and Chris Botting are with the Delta-Q Technologies Corporation, Burnaby, BC V5G 3H3, Canada (e-mail: mcraciun@delta-q.com; cbotting@delta-q.com).

Color versions of one or more of the figures in this article are available online at https://ieeexplore.ieee.org.

Digital Object Identifier 10.1109/TPEL.2020.3006422

Due to the desirable features of *LLC* resonant converters, including high efficiency and reliability, they are considered an attractive power architecture option for battery charger applications and are studied thoroughly in the literature [2]–[5]. Half-bridge and full-bridge *LLC* resonant converters are studied for low power to medium power applications (level 1 charging). For medium to high power level chargers, the three-phase *LLC* structure is an attractive option. Different three-phase resonant converters have been presented in [6]–[11]. Compared to half-bridge and full-bridge structures, three-phase *LLC* resonant converters can provide higher efficiency at increased power levels, automatic current sharing, lower output capacitor current ripple, better thermal distribution, and smaller filter and heat sink size (higher power density). Due to these features, three-phase *LLC* resonant converters are suitable for high-power battery charger applications (levels 2 and 3 chargers) [12].

Although there has been substantial research and development on single-phase *LLC* resonant converters, the literature investigating three-phase *LLC* structures has been limited and emerging. Some important issues with three-phase *LLC* resonant converters are as follows: 1) the natural limited gain range of the *LLC* resonant converter structure, 2) poor light-load efficiency of the converter and possible phase-shedding strategies. Fig. 1 shows how these two issues limit the performance of the converter in a battery charger application. As shown, there are typically three main phases in charging a battery: recovery stage (precharge), bulk charging (constant current), and absorption (constant voltage). The recovery stage usually happens when the battery is overused or has been stored for a long time. In this situation, the battery is in the dead zone and needs to be recovered before the bulk charging starts. This is also called the precharge stage, and low voltage and low current are required to recover the battery.

Due to the natural limited gain range of *LLC* converters, it is a challenge to be able to provide the low voltage and low current needed when designing the converter. For that reason, the precharge stage is considered to be the most difficult stage in a charging cycle [13]. The conventional method to overcome this issue in *LLC* resonant converters is to employ burst mode operation to provide low output voltages at light-load conditions [14]. However, this approach is not desired due to complicated implementation, high electromagnetic interference, and the very high low-frequency output current and voltage ripples introduced to the battery terminals, which drastically affects the battery life. Many different modifications on single-phase *LLC* resonant

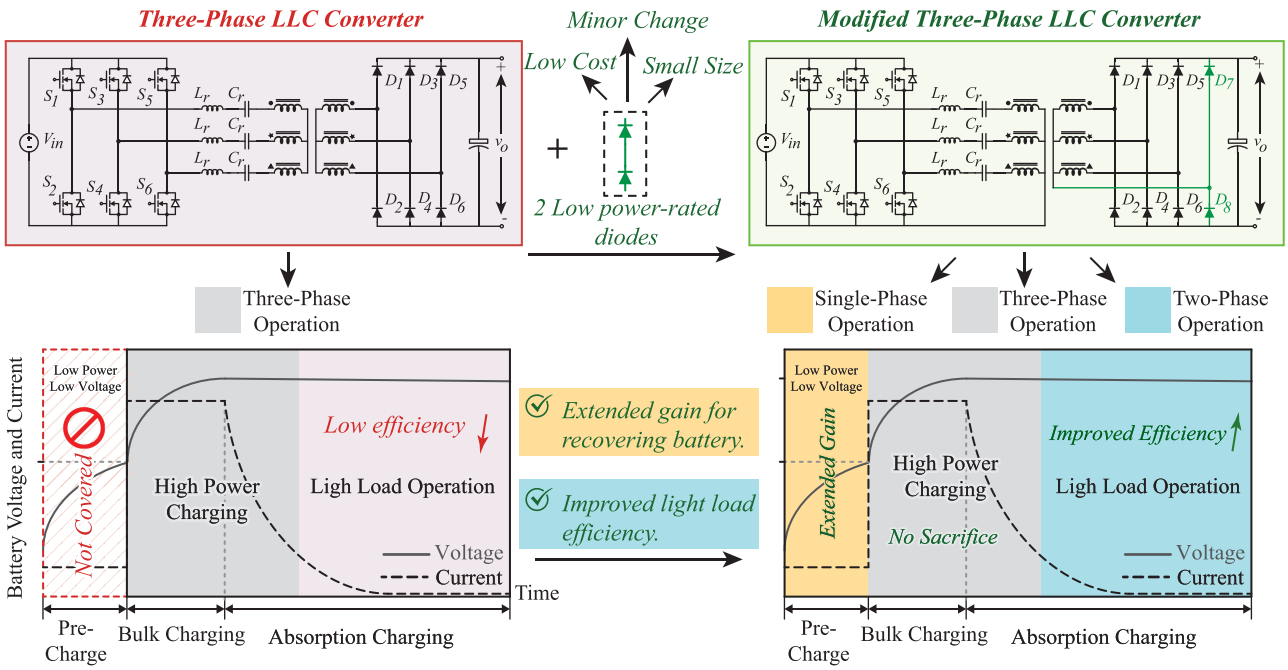

Fig. 1. Proposed modified three-phase *LLC* resonant converter. Compared to a conventional three-phase *LLC* converter, the modified topology has two more small, low power rated diodes. The proposed modified converter provides two-phase and single-phase operations of the circuit. These provide light-load efficiency improvement, and extended gain range for covering the dead zone charging of a battery, receptively.

converters have been investigated to achieve a wide-voltage gain range of the converter [15]. These works include modifications on resonant tanks [16]–[20], reconfiguring primary-side switch network and modulations [21]–[23], integrated topologies [24], [25], and configurations on the secondary-side rectifiers [26]–[30]. Other works, such as adopting a variable dc-link voltage [31], reconfigurable dual LLC converter [32], and adopting two-level turns-ratio transformer [33], have also been presented to achieve extended gain range charger with single-phase and dual *LLC* resonant converters. Although many different solutions are investigated for extending the gain range of single-phase and dual *LLC* resonant converters, no work has been presented on three-phase *LLC* resonant converters.

As mentioned above, the other issue with three-phase LLC resonant converters is their poor light-load efficiency. Compared to single-phase structures, three-phase *LLC* resonant converters provide higher efficiency at heavy load conditions by sharing the load through the phases and reducing the current peak values leading to conduction losses reduction. In the lighter load conditions, the switching and circulating power losses become dominant and that results in a poor light-load efficiency for three-phase structures due to the high number of semiconductor devices [34]. In the absorption stage (constant voltage stage), the battery terminal voltage is kept constant and the charge current starts decreasing to very light-load conditions. As the charging current decreases and the converter goes to lighter load conditions, the three-phase structure will not be efficiently charging anymore. The light-load absorption stage happens during much longer time compare to the other charging stages. This makes it even more important to improve the light-load efficiency of the converter, and the power saving over time will be significant. Modular and interleaved structure of three-phase *LLC* converters makes it more challenging to employ phase-shedding strategies with the aim of light-load efficiency improvement.

In this article, a modified three-phase *LLC* resonant converter with a new phase-shedding technique is proposed to address the regulation and light-load performance issues of the converter. These are achieved by proposing single-phase and two-phase operations of the converter, respectively. Compared to the conventional three-phase *LLC* resonant converter, the proposed topology has two additional small, low power rated diodes, as shown in Fig. 1. The proposed technique delivers the whole package of features needed by a three-phase *LLC* resonant converter in a high-power battery charger application. In Section II, the proposed modified three-phase *LLC* resonant converter and phase-shedding strategy are discussed, and Section III discusses the design procedure and requirements. In Section IV, simulation and experimental results of a 3-kW three-phase *LLC* resonant converter are provided to show the validity of the proposed analysis.

II. Proposed Phase-Shedding Strategy

The proposed modified three-phase *LLC* resonant converter to achieve extended gain range and improved light-load operation is shown in Fig. 1. As mentioned in the previous section, in the modified converter two small low power rated diodes are added to the secondary side of the conventional three-phase *LLC* resonant converter. The proposed converter has three operating modes: three-phase mode [see Fig. 2(a)], two-phase operating mode [see Fig. 2(b)], and single-phase mode [see Fig. 2(c)]. As explained in Fig. 2, with single-phase operation the recovery zone of charging is covered, three-phase mode is used for the bulk charging period, and two-phase operation is for covering the

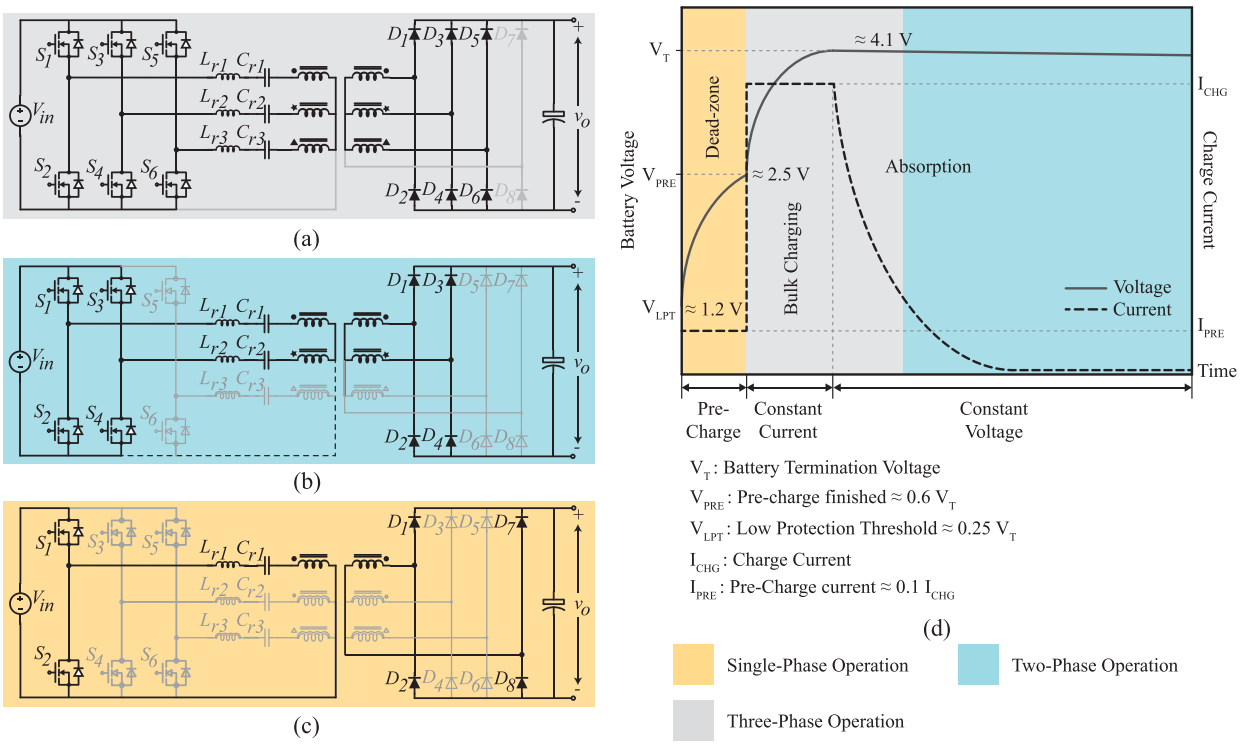

Fig. 2. Proposed phase-shedding strategy. (a) Three-phase operation to cover bulk charging and high power absorption charging. (b) Two-phase operation to cover light-load absorption charging. (c) Single-phase operation to cover the recovering stage, where the battery is fully depleted and low voltage and low current are required for safe charging. (d) Conceptual charging profile of typical Li-ion batteries.

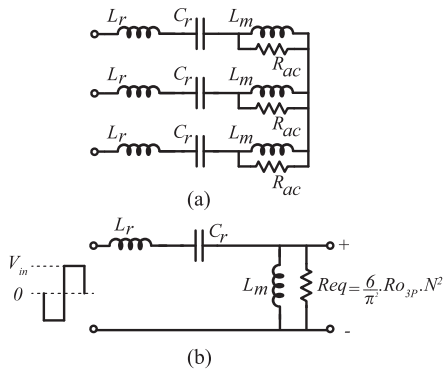

Fig. 3. Equivalent resonant tank circuit of three-phase operation. (a) Resonant tank circuit in operation. (b) Equivalent circuit.

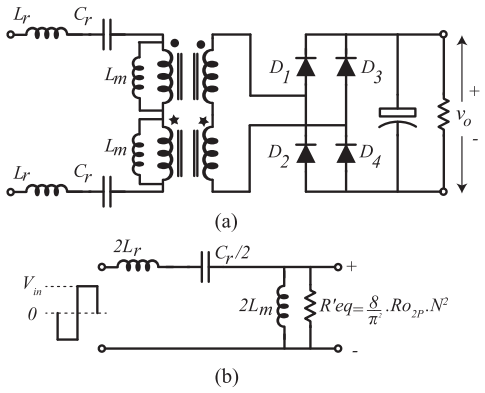

Fig. 4. Equivalent resonant tank circuit of two-phase operation. (a) Resonant tank circuit in operation. (b) Equivalent circuit.

absorption. With these three operating modes, all the charging stages are efficiently covered, as shown in Fig. 2(d). In this section, the three operating modes are analyzed and explained.

A. Operating Modes

The three operating modes of the proposed modified converter are shown in Fig. 2(a)–(c). Using first harmonic approximation and standard analysis principles for resonant converters, the equivalent circuits of the three operating modes of the converter can be derived as in Figs. 3–5.

1) Three-Phase Operation: The three-phase operation happens when the three switching legs are operating phase shifted by 120°. In this situation, the converter operates as a normal

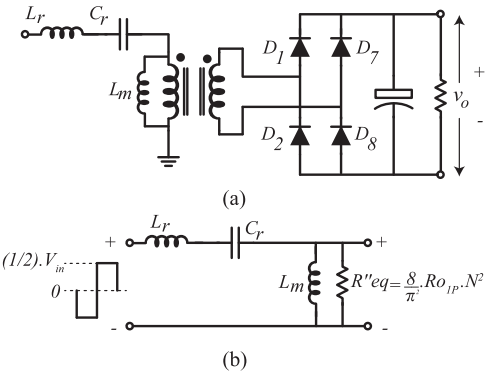

Fig. 5. Equivalent resonant tank circuit of single-phase operation. (a) Resonant tank circuit in operation. (b) Equivalent circuit.

three-phase *LLC* resonant converter, as shown in Fig. 2(a). In this mode, the two added diodes ($D7$ and $D8$) are OFF. Three-phase operation of the *LLC* resonant converter is highly desirable for higher power levels. This is because of the unique features provided by three-phase operation in comparison with conventional half-bridge and full-bridge structures. These features are: interleaved operation, significantly reduced output capacitor current ripple, reduced output filter size, more distributed losses, smaller peak current and temperature values, and lower conduction losses at higher power levels and higher efficiency. Relying on these features, the proposed phase-shedding technique uses the three-phase operation of the circuit to cover the high power charging stages of a charging cycle.

The gain of the converter in this mode is the same as the gain of any conventional three-phase *LLC* resonant converter with full-bridge three-phase rectifier. The equivalent circuit of the converter in this mode is as shown in Fig. 3(b) and the gain of the converter is as

$$M_{3P}(h,Q,f_n)=\frac{V_O}{V_{\text{in}}}=\frac{1}{N\sqrt{(1+\frac{1}{h}-\frac{1}{hf_n^2})^2+Q_{3P}^2(f_n-\frac{1}{f_n})^2}} \tag{1}$$

where N is the transformer turns ratio, h is the inductor ratio, f_n is normalized frequency, and Q_{3P} is the quality factor of the three-phase circuit as follows:

$$N=\frac{N_P}{N_S},\quad h=\frac{L_m}{L_r},\quad f_n=\frac{f_s}{f_r},\quad f_r=\frac{1}{2\pi\sqrt{L_r\cdot C_r}}$$
$$Q_{3P}=\frac{Z_{3P}}{N^2R_{\text{eq}}},Z_{3P}=Z_O=\sqrt{\frac{L_r}{C_r}}. \tag{2}$$

R_{eq} is the equivalent load reflected to primary and is as shown in Fig. 3(b) as

$$R_{\text{eq}}=\frac{6}{\pi^2}\cdot Ro_{3P}\cdot N^2 \tag{3}$$

where Ro_{3P} is the output load at three-phase operation.

2) Two-Phase Operation: Two-phase operation happens when one of the phases is shut down and the other two phases are operating complementary at 180° phase shift. In this case, the converter behaves as a full-bridge *LLC* resonant converter. This mode is shown in Fig. 2(b). This mode results in higher efficiency at lighter load conditions compared to three-phase operation mode. This is due to the fact that at lighter load conditions, the switching losses and circulating power losses are dominant. Hence, shedding one of the phases results in lower losses and higher efficiency. The equivalent circuit of this mode is shown in Fig. 4 and the gain of the converter is as follows:

$$M_{2P}(h,Q,f_n)=\frac{V_O}{V_{\text{in}}}=\frac{1}{N\sqrt{(1+\frac{1}{h}-\frac{1}{hf_n^2})^2+Q_{2P}^2(f_n-\frac{1}{f_n})^2}} \tag{4}$$

where

$$Q_{2P}=\frac{Z_{2P}}{N^2R_{\text{eq}}},\quad R_{\text{eq}}=\frac{8}{\pi^2}\cdot Ro_{2P}\cdot N^2,\quad h=\frac{L_m}{L_r}$$
$$f_r=\frac{1}{2\pi\sqrt{L_r\cdot C_r}},\quad Z_{2P}=2Z_O=2\sqrt{\frac{L_r}{C_r}}. \tag{5}$$

The two-phase operating mode is expected to cover a major part of the absorption stage of charging. In that stage, the charger is in constant voltage mode and the charger is supposed to provide the maximum voltage (V_T) at the output. So, in the two-phase operating mode, the voltage gain is supposed to cover an output voltage fixed at V_T at light-load conditions.

3) Single-Phase Operation: The single-phase operation happens when one of the switching legs is running and the other two legs are OFF. In this situation, the current path is closed through the ground connection of the transformer in the primary. At the secondary side, diodes $D7$ and $D8$ form a full-bridge rectifier along with diodes $D1$ and $D2$, as shown in Fig. 2(c). The equivalent circuit of the converter in this mode is as shown in Fig. 5 and the gain of the converter is as:

$$M_{1P}(h,Q,f_n)=\frac{V_O}{V_{\text{in}}}=\frac{1}{2N\sqrt{(1+\frac{1}{h}-\frac{1}{hf_n^2})^2+Q_{1P}^2(f_n-\frac{1}{f_n})^2}} \tag{6}$$

where

$$Q_{1P}=\frac{Z_{1P}}{N^2R_{\text{eq}}},\quad R_{\text{eq}}=\frac{8}{\pi^2}\cdot Ro_{1P}\cdot N^2,\quad h=\frac{L_m}{L_r}$$
$$f_r=\frac{1}{2\pi\sqrt{L_r\cdot C_r}},\quad Z_{1P}=Z_O=\sqrt{\frac{L_r}{C_r}}. \tag{7}$$

As can be seen in Fig. 5(a), in the single-phase operating mode, the converter behaves as a half-bridge *LLC* resonant converter and that is why the input voltage of the resonant tank in Fig. 5(b) is half the voltage value in three-phase and two-phase operating modes. Because of the half-bridge operation, the gain of the converter in the single-phase mode is almost half the value of that in the other two operating modes. This feature provides the low voltage and low current needed for covering the dead zone of battery charging.

B. Phase-Shedding Strategy

The intended outcomes of using a three-phase circuit are to improve power distribution in the circuit and to achieve higher power while maintaining efficiency. At high power levels, the conduction losses dominate the total losses in the circuit. Conduction losses are proportional to the square value of the peak current. Efficiency at high power levels is improved by reducing the peak conducting current by sharing the current between the three phases in the circuit. For these reasons, the three-phase operation is desirable for bulk charging and some high power charging portions of the absorption stage. With the three-phase operation, the converter is expected to cover the output voltage range from V_{PRE} to V_T at different loading conditions from

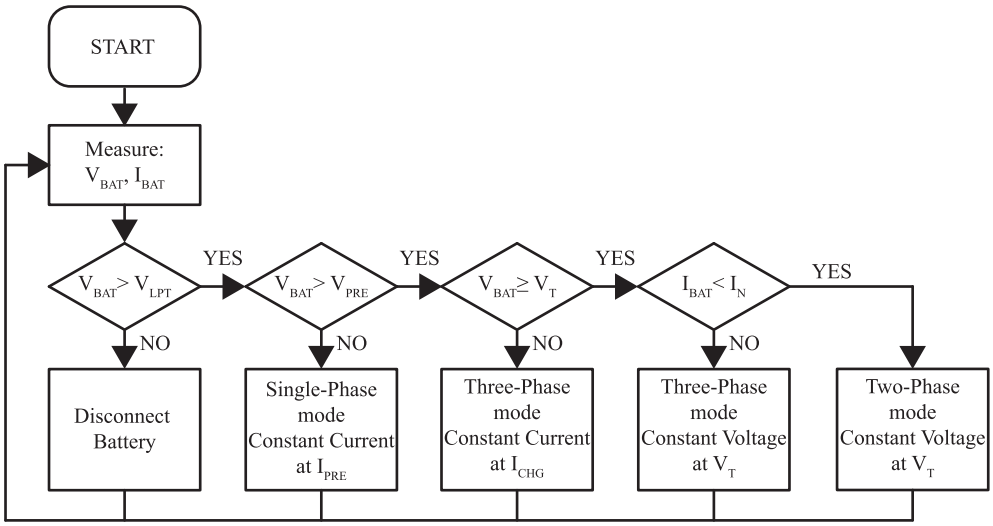

Fig. 6. Conceptual flowchart of phase-shedding strategy in the proposed modified three-phase *LLC* resonant converter.

maximum current (I_{CHG}) to I_N (where the three-phase mode will be switched to two-phase mode).

The problem within three-phase converters is that the efficiency drops at low power levels. That is due to the fact that, at low power levels, the switching losses, gate driving circuits losses, and circulating currents losses dominate the total losses in the power stage. Efficiency improvement in low power levels can be achieved through phase-shedding. Phase-shedding for the three-phase resonant converter is achieved by using two-phase operation, as discussed earlier. In this operation mode, one of the phases is shut down and carries no load, no circulating current, and no switching and driving losses. That leads to improved efficiency at light-load conditions and considerable power saving over time. As mentioned earlier, in the two-phase operating mode, the converter must provide the maximum output voltage (V_T) from I_N to very light-load conditions.

When the converter operates in the single-phase mode, the gain of the converter is reduced to almost half the value compared to the other two modes. With single-phase operation, the low voltage and low current needed for the recovery mode can be easily provided. Due to the low current in the recovery mode, the two added diodes ($D7$ and $D8$) are small low rated diodes. Moreover, since the recovery mode is supposed to happen at one tenth of the nominal power, the single-phase operation can easily take that power.

Considering the abovementioned features of the three-operating modes, the phase-shedding strategy for battery charging is shown in Fig. 6. This flowchart shows how the phase-shedding strategy works as it is defined in Fig. 2(d).

C. Power-Loss Analysis

The intended outcome of two-phase operation is achieving higher efficiency at low-power absorption charging. The following analysis is to mathematically prove the higher efficiency of two-phase operation compared to three-phase operation at low power levels.

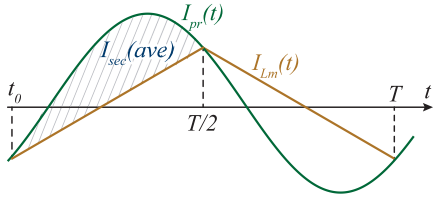

Fig. 7. Subtraction of the total primary current and magnetizing current reflects the power transferred to the load.

1) Conduction Losses: These part of losses are investigated as primary losses and secondary losses.

a) Primary conduction losses: For the primary conduction losses, the root mean square (rms) values of the primary currents is needed. Fig. 7 conceptually shows how the primary current and the magnetizing current look like. The peak value of the magnetizing current in both three-phase mode and two-phase mode are equal and can be determined as

$$\begin{cases} I_{Lm}(\mathrm{Peak}) = \frac{\frac{N_P}{N_S}\times\frac{V_O}{2}}{2.L_m} \times \frac{T}{2} = \frac{\frac{N_P}{N_S}\times\frac{V_O}{2}}{8.L_m.f_{\mathrm{sw}}} \\ I_{\mathrm{pr}}(t) = \sqrt{2} I_{\mathrm{rms}} \sin(\omega) \\ \qquad \longrightarrow I_{\mathrm{pr}}(t_0) = \sqrt{2} I_{\mathrm{rms}} \sin(\phi) = -\frac{NV_O}{8L_m f_{\mathrm{sw}}}. \end{cases} \tag{8}$$

As depicted in the figure, the difference between the primary and magnetizing current is equal to the transferred current to the secondary side. Therefore

$$\frac{2}{T}\int_0^{\frac{T}{2}} (i_{\mathrm{pr}}(t) - i_{Lm}(t))dt = \frac{I_{\mathrm{sec}}(\mathrm{ave})}{N} \tag{9}$$

where $I_{\mathrm{sec}}(\mathrm{ave})$ is the average current in the secondary side of the transformers and is given as in the following equation, in the different operating modes

$$\begin{cases} \text{Two-Phase Operation} \\ \qquad\qquad I_{\mathrm{sec}}(\mathrm{ave}) = I_O \\ \text{Three-Phase Operation} \\ \qquad\qquad I_{\mathrm{sec}}(\mathrm{ave}) = 2I_O/3. \end{cases} \tag{10}$$

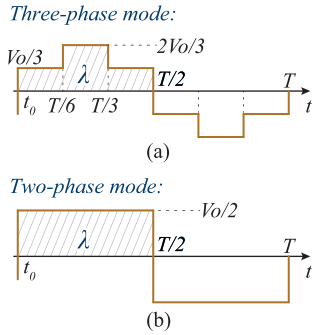

Fig. 8. Volt–second of the secondary side of the transformers in: (a) three-phase mode, (b) two-phase mode.

Now, by solving (9), the rms values of the primary currents in both operating modes can be found as

$$\begin{cases}\text{Two-Phase Operation}\\ I^2_{\text{pr},3P}(\text{rms}) = (\frac{\pi^2}{8N^2}) \times I_O^2 + \frac{N^2}{64\times 2\times L_m^2\times f^2} \times V_O^2\\ \text{Three-Phase Operation}\\ I^2_{\text{pr},2P}(\text{rms}) = \frac{4}{9} \times (\frac{\pi^2}{8N^2}) \times I_O^2 + \frac{N^2}{64\times 2\times L_m^2\times f^2} \times V_O^2.\end{cases} \tag{11}$$

As it can be seen in (11), there are two terms that determine the total rms value of the primary currents. The first term is a function of output current (I_O), which determines the transferred power. The other term is a function of output voltage, which determines the circulating power generated by the magnetizing inductor. Using these values, the total primary conduction losses of both operating modes can be estimated as

$$\begin{cases}\text{Two-Phase Operation}\\ P_{\text{cond,pr}} : 2 \times I^2_{\text{pr},2P}(\text{rms}) \times (R_{\text{DS,ON}} + R_L + Rw)\\ \text{Three-Phase Operation}\\ P_{\text{cond,pr}} : 3 \times I^2_{\text{pr},3P}(\text{rms}) \times (R_{\text{DS,ON}} + R_L + Rw)\end{cases} \tag{12}$$

where $R_{\text{DS,ON}}$, R_L, and Rw are the parasitic resistances of the MOSFETs, inductors, and transformer's windings, respectively. The ac resistance of the inductors and transformers can also be integrated in the values of R_L, and Rw. Fig. 9(a) conceptually shows the trend of the primary conduction losses in both two-phase and three-phase operating modes. As it can be seen, there are lower primary conduction losses in two-phase operation at light load conditions. However, by moving to heavy load the losses in two-phase operation increases exponentially.

b) Secondary conduction losses: There are the following two different losses associated with the secondary side conduction losses: 1) losses associated with the voltage drop of diodes, and 2) losses associated with the internal resistance of diodes.

1) Losses associated with the voltage drop of diodes: To estimate this loss, the average value of the current through diodes needs to be taken into account. The average current through diodes in both operating modes can be found as following:

$$\begin{cases}\text{Two-Phase Operation :} & I_D(\text{ave}) = I_O/2\\ \text{Three-Phase Operation :} & I_D(\text{ave}) = I_O/3.\end{cases} \tag{13}$$

The abovementioned values are derived based on the fact that in the three-phase operation, the peak value of the diodes is equal to $I_O \times \pi/3$. However, in two-phase operation, the peak value of diodes is equal to $I_O \times \pi/2$. Using the values in the abovementioned equation, the total loss can be estimated as

$$\begin{cases}\text{Two-Phase Operation}\\ P_{\text{cond,sec}_1} : I_D(\text{ave}) \times V_{D,\text{ON}} \times 4 = 2 \times I_O \times V_{D,\text{ON}}\\ \text{Three-PhaseOperation}\\ P_{\text{cond,sec}_1} : I_D(\text{ave}) \times V_{D,\text{ON}} \times 6 = 1.9 \times I_O \times V_{D,\text{ON}}.\end{cases} \tag{14}$$

Fig. 9(c) conceptually shows the trend of this loss in both operating modes.

2) Losses associated with the parasitic resistances: For calculating this part of losses, the rms values of the currents through diodes is required. These values can be calculated as

$$\begin{cases}\text{Two-Phase Operation :} & I_D(\text{rms}) = I_O \times \pi/4\\ \text{Three-Phase Operation :} & I_D(\text{rms}) = I_O \times \pi/6.\end{cases} \tag{15}$$

The total losses associated with this part in both operating modes can be estimated as

$$\begin{cases}\text{Two-Phase Operation}\\ P_{\text{cond,sec}_2} : 4 \times R_D \times I^2_{D,\text{rms}} = 2.47 \times R_D \times I_O^2\\ \text{Three-Phase Operation}\\ P_{\text{cond,sec}_2} : 6 \times R_D \times I^2_{D,\text{rms}} = 1.65 \times R_D \times I_O^2.\end{cases} \tag{16}$$

In Fig. 9(b), the trend of these losses are depicted, conceptually. By adding the values of (14) and (16), the total losses associated with secondary conduction losses can be estimated. As it can be seen, this loss increases exponentially with increasing the load. Moreover, the losses in the two-phase circuit is always higher than in the three-phase circuit. Although, this difference is not considerable at low output currents, it becomes significant as the converter moves to higher power levels.

2) Magnetic Losses: These losses are associated with the inductors and transformer.

a) Transformers' core Losses: The core losses of a magnetic component is calculated using the following equation:

$$P_{\text{core}} = k_{fe} f_{\text{sw}} (\Delta B)^{\beta} A_C l_m \tag{17}$$

where k_{fe} is a constant, and the typical values of β for ferrite is around 2.6 or 2.7. ΔB is the maximum flux swing, A_C is the cross sectional area of the core, and l_m is the length of the magnetic path. Except for ΔB, other parameters in the equation mentioned above are based on the core geometry and are equal in both operating modes. The maximum flux swing in both operating modes can be found using the volt–second relation of the transformers. Fig. 8 shows the secondary voltage of the

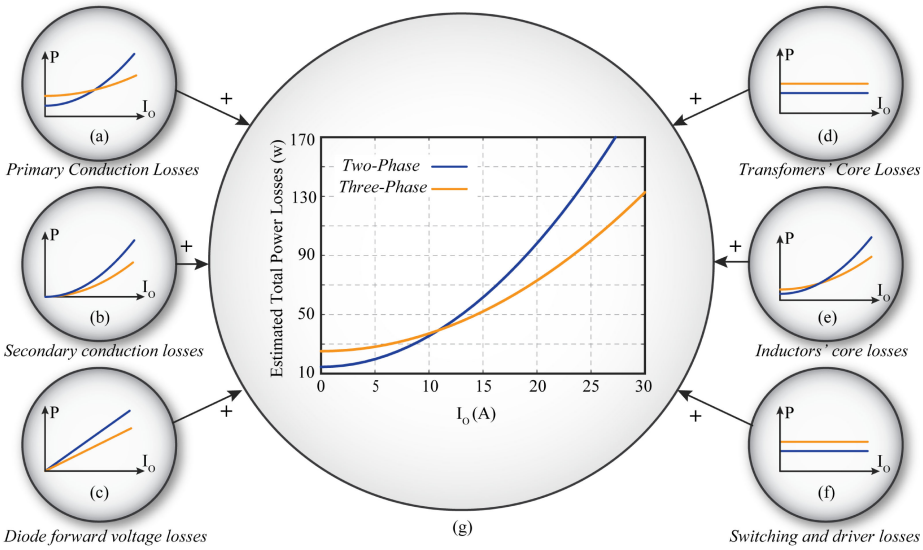

Fig. 9. Breakdown of the total estimated power loss over the output current range at constant output voltage. (a) Primary conduction losses ($P_{\text{cond,pr}}$). (b) Secondary conduction losses ($P_{\text{cond,sec}_2}$). (c) Diodes forward voltage drop losses ($P_{\text{cond,sec}_1}$). (d) Transformers core losses ($P_{\text{core,Tr}}$). (e) Inductors core losses ($P_{\text{core},L}$). (f) Switching losses (P_{sw}) (g) Total power loss.

TABLE I
DESIGN WORST CASE CONDITIONS

Operating mode	Case	Gain	Worst case condition
Three-Phase	I	$M_{3P,Max}$	Q_{Max} @ $R_{O,Min}=\frac{V_T}{I_{CGH}}$
	II	$M_{3P,Min}$	Q_{Min} @ $R_{O,Max}=\frac{V_{PRE}}{I_{CGH}}$
Two-Phase	III	$M_{2P,Max}$	Q_{Max} @ $R_{O,Min}=\frac{V_T}{I_N}$
Single-Phase	IV	$M_{2P,Max}$	Q_{Max} @ $R_{O,Min}=\frac{V_{PRE}}{I_{PRE}}$
	V	$M_{3P,Min}$	Q_{Min} @ $R_{O,Max}=\frac{V_{LPT}}{I_{PRE}}$

transformers in both operating modes. Therefore,

$$\begin{cases}\text{Two-Phase Operation}\\ \qquad B_{\max}=\frac{\int_0^{\frac{T}{2}} v_{\text{tr}}dt}{2N_sA}=\frac{V_O}{8f_{\text{sw}}AN_s}\\ \text{Three-Phase Operation}\\ \qquad B_{\max}=\frac{\int_0^{\frac{T}{2}} v_{\text{tr}}dt}{2N_sA}=\frac{V_O}{8f_{\text{sw}}AN_s}.\end{cases}\tag{18}$$

As can be seen in the abovementioned equation, transformers in both operating modes experience the same flux variations. This means the same value of loss per transformers in both operating modes. However, the total transformer core loss for the three-phase operation would be $\frac{3}{2}$ times higher than two-phase operation, as there are three transformers under operation in three-phase circuit. This can be stated as

$$\text{Total } P_{\text{core,Tr},3P}=\frac{3}{2}\,\text{Total } P_{\text{core,tr},2P}.\tag{19}$$

This losses is almost independent from loading conditions. In Fig. 9(d), these losses are depicted, conceptually.

b) Inductors core losses: As mentioned above, the core losses of magnetic components are calculated using (17). In an inductor, the maximum flux swing is proportional to the peak current of the inductor and is calculated as

$$B_{\max}=\frac{LI_{L,\text{peak}}}{NA}\tag{20}$$

The peak value of the current in the inductors is equal to the peak current of the primary current and is as

$$\begin{cases}\text{Two-Phase Operation}\\ \qquad I_{L,\text{Peak}}=\sqrt{2}\times I_{\text{pr},2P}(\text{rms})\\ \text{Three-Phase Operation}\\ \qquad I_{L,\text{Peak}}=\sqrt{2}\times I_{\text{pr},3P}(\text{rms}).\end{cases}\tag{21}$$

As expected, the primary current peak value is higher for two-phase operation at heavier loads compared to three-phase operation. Using the values in the abovementioned equations and (17), the relationship between the total inductor core losses in two-phase operation and three-phase operation can be estimated as

$$\text{Total } P_{\text{core},L,2P}=\frac{2}{3}\times\left(\frac{I_{L,\text{Peak},2P}}{I_{L,\text{Peak},3P}}\right)^{\beta}\times\text{Total } P_{\text{core},L,3P}.\tag{22}$$

Despite the transformers core losses, the total inductor core losses have a different behavior. In the very light-load conditions, the primary peak current values are equal for both operating modes and that results in higher inductor loss for the three-phase operation. However, as the load current increases, the peak current value for the two-phase operation exponentially exceeds the value in three-phase operation. This results in a higher total inductor loss in two-phase operation at heavier load conditions. Fig. 9(e) shows the conceptual trend of this loss.

3) Switching and Gate-Driver Losses: Since the *LLC* converter provides zero-voltage-switching (ZVS) at turn-ON, there

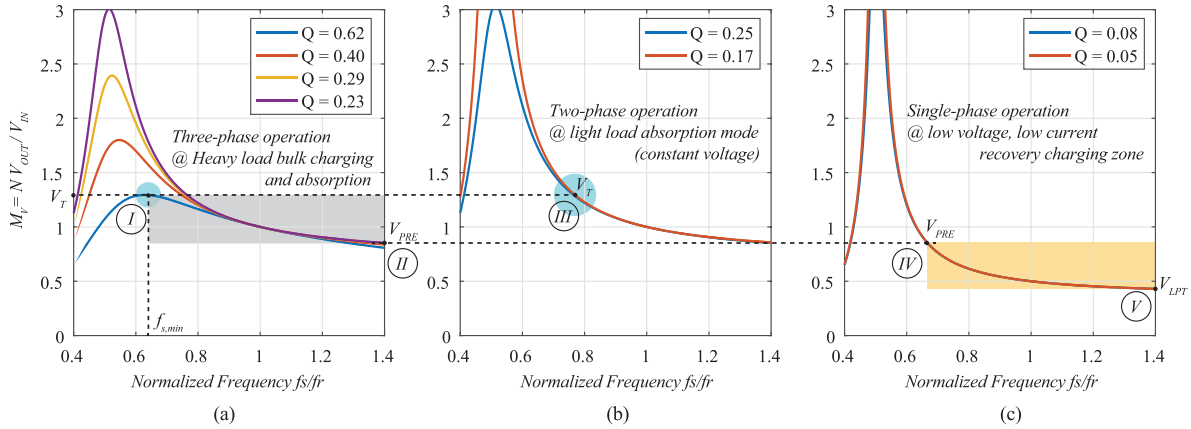

Fig. 10. Normalized gain curves of the different operating modes, where $h = 3$. (a) Three-phase operating mode. (b) Two-phase operating mode. (c) Single-phase operating mode. The color shaded areas show the charging states are covered by different operating modes as explained in Fig. 2(d), and I, II, III, IV, and V are the worst case design conditions as explained in Table I.

is negligible turn-ON losses. The remained sources of switching losses are associated with turn-OFF and gate-drive losses. Turn-OFF happens at $I_{Lm}(\text{peak})$, which is equal at both operating modes and is as (8). Therefore, the switching loss can be estimated as

$$P_{\text{sw}} = \frac{1}{2} V_{\text{in}} I_{Lm} f t_{\text{dis}} = \frac{1}{2} V_{\text{in}} \frac{N V_O}{8 L_m} \times t_{\text{dis}} \tag{23}$$

where t_{dis} is the discharge time of the MOSFET parasitic capacitance, and is calculated as

$$t_{\text{dis}} = \frac{2 C_{\text{eq}} V_{\text{in}}}{I_{Lm}}. \tag{24}$$

As can be seen from the abovementioned equations, the turn-OFF losses are independent from the load current. This is the same for the gate-drive losses. Hence, the total switching losses are equal to the calculated numbers times the number of active switches. The relation between the total switching losses in both operating modes can be stated as

$$\text{Total } P_{\text{sw},2P} = \frac{2}{3} \times \text{Total } P_{\text{sw},3P}. \tag{25}$$

Fig. 9(f) shows the relation between the switching losses of two-phase and three-phase operating modes.

The total estimated power losses is derived by adding the different calculated losses mentioned above. Fig. 9(g) shows the total estimated losses within two-phase and three-phase operating modes. Based on this, a higher efficiency is expected in two-phase operation at light-load conditions.

III. Design Procedure

The goal of this section is to see how the three operating modes of the proposed modified converter are able to cover the design requirements of a battery charger application and to explain the design procedure. Resonant tank design of resonant converters is the most challenging part of the design. The first step for the resonant tank design is looking into the characteristics of the equivalent resonant tanks of the three operating modes. As can be seen from (2), (5), and (7), the resonant frequencies of the resonant circuits do not change for the three-phase, two-phase, and single-phase operating modes of the converter. Moreover, the ratio of the parallel inductor value to the series inductor value (h) is equal for all the operating modes. These two parameters are critical in designing *LLC* resonant converters and determining the frequency and gain range of the converter. The gain of the dc–ac inverter bridge, which basically determines the dc gain of the converter at resonant frequency (f_r), is unity for both the three-phase and the two-phase operating modes. However, in the single-phase operating mode, the dc–ac stage delivers half the gain compared to the three-phase and two-phase operating modes, as mentioned in the previous section. Comparing (2), (5), and (7), there are slight differences in the values of the impedance and the equivalent reflected load of the equivalent resonant circuits of the three operating modes. These two parameters define the quality factors of the equivalent resonant tanks' circuits and have an impact on the gain curves of the converter.

So, the design of the converter needs to be optimized based on the minimum and maximum values of the quality factor for different operating modes. In order to do that, the worst case scenarios that need to be considered in designing the converter are defined as in Table I. These worst case conditions are defined based on the maximum and minimum gains required in different operating modes. As shown in Fig. 2(d), the three-phase operating mode needs to cover the output voltage from V_{PRE} to V_T at heavy-loads to light-load conditions. Then, in the two-phase operating mode, the output voltage will be fixed at V_T for light-load to no-load conditions. The case for the single-phase operating mode is a bit different. In the single-phase operating mode, the output voltage varies from V_{LPT} to V_{PRE} at a fixed low output current (I_{PRE}). Table I summarizes this information. In Fig. 10, the normalized gain curves of the three operating modes are depicted, based on the design shown in Table II. The gain curves of the different operating modes correspond to the maximum and minimum values of quality factors as explained in Table I.

The *LLC* resonant converter's design has been studied in details in the literature [2]–[5]. The design rule check flowchart of the proposed modified converter is shown in Fig. 11. Based on the fact that the two-phase and single-phase operations of the converter happen at fairly light-load conditions with low numbers for the quality factors, the gain requirements of those operating modes would possibly be met if the converter was

TABLE II
DESIGN PARAMETERS OF THE EXPERIMENTAL SETUP

Parameter	Values
V_{in}	$400V$
$V_{out,nom}$	$96V$
$P_{out}(max)$	$3kW$
V_T	$100V$
V_{PRE}	$60V$
V_{LPT}	$32V$
I_{CHG}	$30A$
I_{PRE}	$3A$
n_1/n_2	$16/3$
f_r	$205kHz$
h	3
L_r	$20\mu H$
C_r	$30nF$
L_m	$60\mu H$

properly designed for the three-phase operating mode. This can be observed in the plots in Fig. 10. However, this also depends on the design requirements, such as V_{PRE}, V_{LPT}, I_{CHG}, and I_{PRE}. For that reason, the design needs to be verified for the different operating modes. Based on that, the first step in the design procedure of the proposed modified three-phase *LLC* resonant converter is to design a basic three-phase *LLC* resonant converter, as explained in [9] and [12]. Once the resonant tank is preliminary designed, the design rule checking, as shown in Fig. 11, needs to be done. In this flowchart, the worst conditions defined in Table I are targeted. First, the conditions for the three-phase mode are verified, and then it proceeds to the two-phase and single-phase modes, respectively. Once the requirements for all the worst conditions are met, the design is passed.

Turn-ON soft switching is the other important design consideration, which is determined with the switch-ON current. Switch-ON current is equal to the magnetizing peak current (I_{Lm}(Peak)). Discharging the MOSFET junction capacitor happens at that current and if enough dead-time is ensured, ZVS at turn-ON will be achieved (please refer to Section II-C2). As indicated in (8), the magnetizing peak current in all the operating modes are equal. Therefore, if ZVS is ensured for the three-phase operation, changing the operation mode does not affect the turn-ON ZVS.

A significant advantage of the three-phase operation is the output capacitor current ripple reduction, which is due to the interleaved operation of the phases. This feature enables the use of a much smaller output capacitor (compared to a single-, or two-phase solution), which is particularly beneficial for high current outputs since the required capacitance is proportional to the load current. However, when the converter switches to two-phase and single-phase operation, the ripple cancellation benefit is lost. Output capacitor current ripple for the three-phase and two-phase operating modes are given by the following equation:

$$\Delta i_c = \left(1 - \frac{\sqrt{3}}{2}\right) \cdot \frac{\pi}{3} \cdot I_O \approx 0.14 \times I_O \tag{26}$$

$$\Delta i_c = \frac{\pi}{2} \cdot I_O \approx 1.57 \times I_O \tag{27}$$

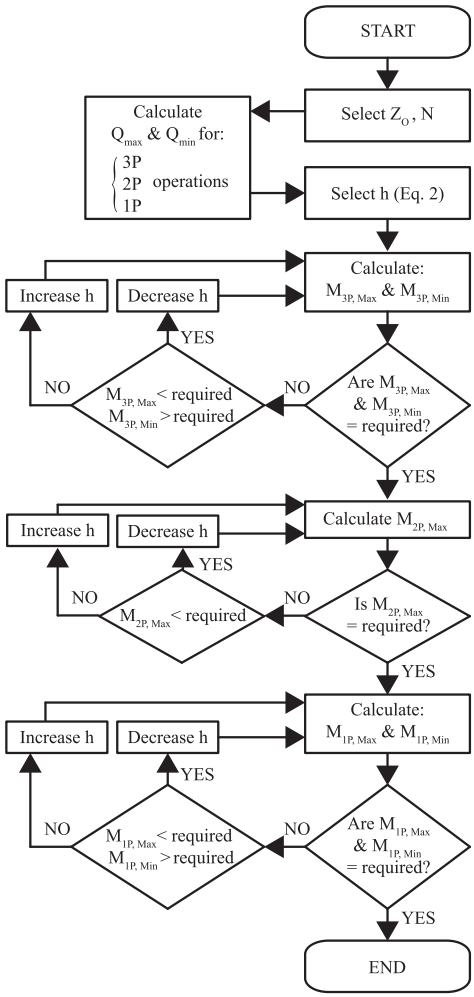

Fig. 11. Design rule checking.

where I_O is the output current mean value. As can be seen, for the same output current mean value, the output capacitor current ripple in the two-phase operating mode is more than 10 times greater than the ripple in the three-phase operating mode. Depending on the point where the switch from three-phase mode to two-phase mode happens, the capacitance needs to be sized according to the maximum two-phase load current in a given design. Hence, the value of the output capacitor must be determined based on the power value that the converter operating mode is switched to the two-phase mode.

As mentioned earlier, the two added diodes $D7$ and $D8$ only operate in the single-phase operating mode, where the output current is equal to I_{PRE}, around one-tenth of I_{CHG}. Therefore, these two diodes are rated at much smaller values compared to the other six diodes.

IV. EXPERIMENTAL RESULTS

In order to verify the extended gain range and improved light-load operation of the proposed phase-shedding strategy, a 3-kW prototype was developed and tested under different operating conditions. The specifications of the developed converter are shown in Table II. The converter is designed for charging a Li-ion battery pack consisting of a series connection of 24 battery

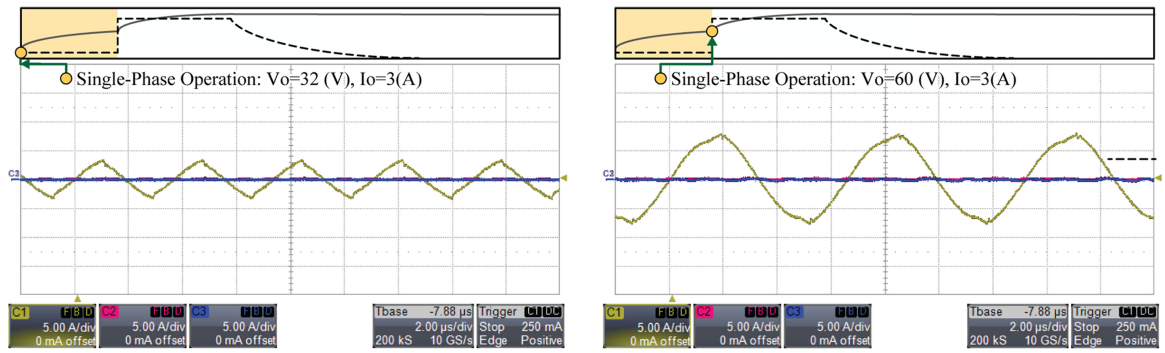

Fig. 12. Experimental results of the single-phase operating mode: Primary currents waveforms. With single-phase operation, the recovery stage of charging can be covered without the need for burst mode operation.

TABLE III
COMPONENTS SUMMARY

Component	Part number
MOSFETs	$IPP60R190P6$
Diodes D1-D6	$STPS20120D$
Diodes D7&D8	$V3FM12$
Transformers core	$E42/21/20$
Inducotrs core	$RM14$

cells. The nominal output voltage of the converter is 96 V and V_{LPT} and V_{PRE} are 32 V and 60 V, respectively. The maximum charging current (I_{CHG}) is 30 A, and the precharge current I_{PRE} is 3 A. Based on this design, the converter is expected to cover the output voltages of 32–100 V. Table III summarizes the important selected components. As can be seen, diodes $D1$–$D6$ package is TO-220, however, $D7$ and $D8$ package is DO-219AD, which is a much smaller surface-mount package.

A. Operating Modes

Considering the charging profile in Fig. 2 and the design parameters in Table II, the converter will have the following operating modes and conditions.

1) Single-Phase Operating Mode: This mode covers the precharge stage of charging. It means that the converter in this mode must be able to provide output voltages from 32 to 60 V at an output current of 3 A. The experimental results of the single-phase operation are shown in Fig. 12. As the experimental results show, the converter is able to cover the precharge stage. In this mode of operation, the current through two of the phases is zero and only one of the phases is operating. Diodes $D1$, $D2$, $D7$, and $D8$ form the output rectifier of the converter in this mode. As explained earlier, diodes $D7$ and $D8$ are much smaller rated diodes compared to the other six diodes and they only operate in the single-phase operation.

2) Three-Phase Operating Mode: This mode of the converter must be able to cover the bulk charging and absorption stages of the charging profile. Referring to Fig. 2 and Table II, the three-phase operation should provide output voltages from 60 to 100 V at 30 A output current in the bulk charging stage, and 100 V output voltage at light-load conditions to full-load in the absorption stage. Fig. 13 presents the experimental results of the converter at the three-phase operation. The experimental results validate that the converter meets the design requirements of bulk and absorption charging in the three-phase operation. As explained earlier, in this mode, the converter behaves as a normal three-phase *LLC* resonant converter, and diodes $D7$ and $D8$ will not be conducting.

3) Two-Phase Operating Mode: When the charging profile goes to the light-load conditions of the absorption stage, the two-phase operating mode is expected to provide higher efficiency. Improved efficiency at the light-load condition in the absorption stage is important because this part of charging takes much longer than the other stages of charging. Hence, the power savings over time are highlighted. The experimental results of the two-phase operation are shown in Fig. 14. As the results show, in this mode the converter can cover the light-load to mid-load conditions of the absorption charging. In order to confirm the improved light-load efficiency of the two-phase operation, the efficiency curves of both three-phase and two-phase operations are plotted in Fig. 15. The results clearly validate the higher efficiency of the two-phase operation at the light-load absorption stage. The efficiency improvement is around 5% at 100 W and almost 1% at 500 W. This also verifies the power-loss analysis presented in Section II-C and the trend in Fig. 9.

B. Phase-Shedding Transition

The transition between the operating modes happens in the following sequence.

1) Transition From Single-Phase Operation to Three-Phase Operation: This transition happens when the low-power precharge has been done and the bulk charging needs to be started. A noninterrupted power delivery is not required for this transition. This is why burst-mode operation is allowed for the precharge mode. This means that when the precharge is done, the converter can be restarted to start bulk-charging with the three-phase operating mode. This is done through a handshaking protocol between the battery management system (BMS) and the charger. In the case of transition from single-phase operation (precharge) to three-phase operation (bulk charging), restarting the converter takes less than few milliseconds, which is not considered as an issue compared to the total hours of charging process. The stabilized operation of the converter in this transition is inherent.

2) Transition From Three-Phase Operation to Two-Phase Operation: This transition happens when the constant-current

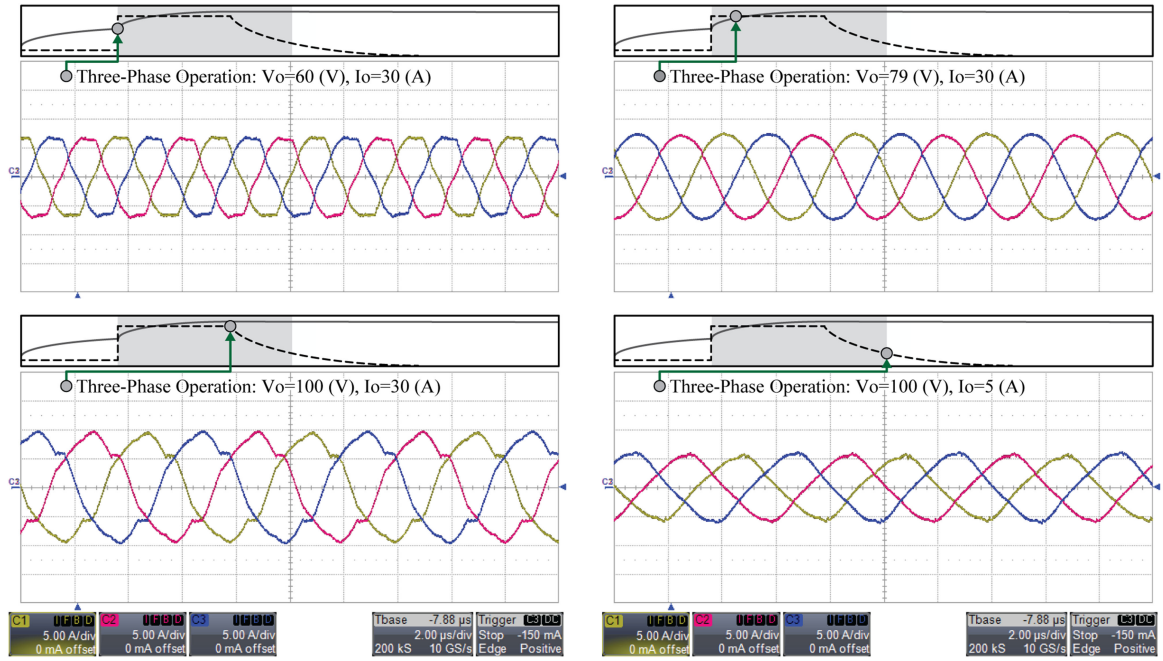

Fig. 13. Experimental results of the three-phase operating mode: Primary currents waveforms at 60, 79, and 100 V output voltage. The three-phase operation efficiently covers the bulk and absorption stages of the charging profile.

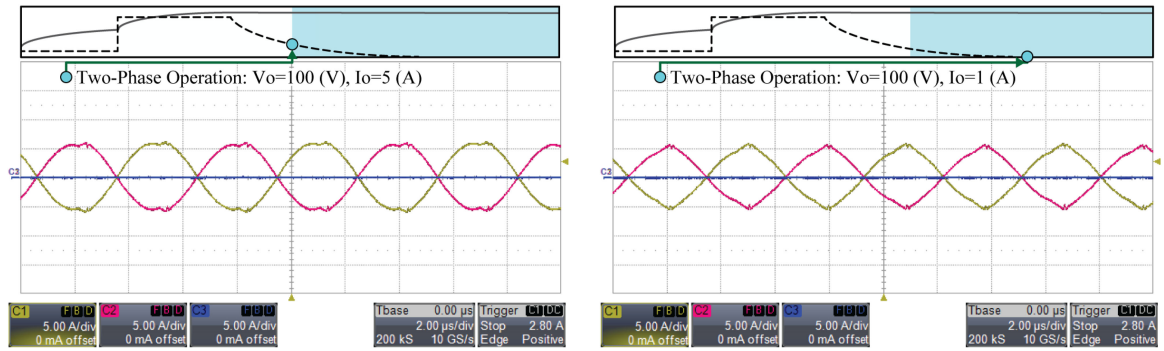

Fig. 14. Experimental results of the two-phase operating mode: Primary currents waveforms at 100 V output voltage, and from light-load condition to half load. In this mode, the two phases are operating at 180° phase shift. The two-phase operation mode covers the lighter load part of the absorption stage of charging cycle with a higher efficiency compared to the three-phase operating mode (see Fig. 15).

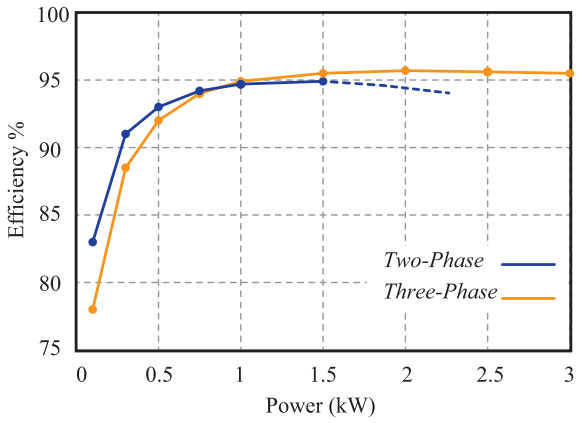

Fig. 15. Efficiency curves of two-phase operation versus three-phase operation. This test has been done at the maximum output voltage ($V_o = 100$ V). Light-load efficiency improvement by two-phase operation is evident.

charging (bulk charging) and most of the constant-voltage (absorption) has been passed, and the converter is entering the low-efficiency light-load absorption charging at maximum output voltage. This is where the two-phase operation offers a higher efficiency as depicted in Fig. 15. Despite the transition from precharge to bulk-charging mentioned above, here an uninterrupted power delivery is preferred as it may cause some confusions for the BMS. Based on the analysis provided in the Section II-A, the two-phase and three-phase operating modes of the converter have very similar behavior characteristics at light load conditions, which allows a very soft transition between the modes. The transition is simply done by shutting down one of the phases and phase shifting the other two switching legs from 120° to 180° at the same time. Fig. 16 shows the experimental result of the transition of the converter from three-phase operation to two-phase operation at light-load absorption charging. The experimental and simulation results validate the excellent

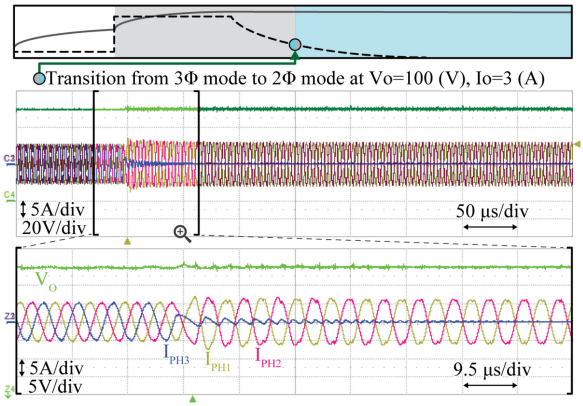

Fig. 16. Experimental result of the transition from three-phase operation to two-phase operation at light-load absorption charging.

stability of the converter during the transition from three-phase operation mode to the two-phase mode. This transition is done at the output current of 3 A, and the output voltage of 100 V.

V. Conclusion

In this article, a modified three-phase *LLC* resonant converter with a new phase-shedding strategy has been proposed. With the aid of two additional small and low power rated diodes, single-phase operation of the converter is realized. Single-phase operation provides an extended gain range that facilitates providing the low voltage and low current needed for recovering a fully depleted Li-ion battery. Moreover, two-phase operation of the converter has been implemented delivering improved light-load efficiency. This leads to significant power saving over time during light-load absorption charging. The design requirements and procedure of the proposed converter were discussed. In order to show the validity of the modified three-phase *LLC* resonant converter and the functionality of the proposed phase-shedding strategy, a 3-kW experimental prototype for charging a 96 V plug-in hybrid electric vehicle (PHEV) battery pack has been developed and tested under different conditions. The results validate the extended gain range and improved light-load efficiency. The proposed converter is able to efficiently cover all the charging stages of a Li-ion PHEV battery pack.

References

[1] M. Yilmaz and P. T. Krein, "Review of battery charger topologies, charging power levels, and infrastructure for plug-in electric and hybrid vehicles," *IEEE Trans. Transp. Electrific.*, vol. 28, no. 5, pp. 2151–2169, May 2013.

[2] R. Beiranvand, M. R. Zolghadri, B. Rashidian, and S. M. H. Alavian, "Optimizing the LLC–LC resonant converter topology for wide-output-voltage and wide-output-load applications," *IEEE Trans. Power Electron.*, vol. 26, no. 11, pp. 3192–3204, Nov. 2011.

[3] C. Hua, Y. Fang, and C. Lin, "LLC resonant converter for electric vehicle battery chargers," *IET Power Electron.*, vol. 9, no. 12, pp. 2369–2376, Oct. 2016.

[4] H. N. Vu and W. J. Choi, "A novel dual full-bridge LLC resonant converter for CC and CV charges of batteries for electric vehicles," *IEEE Trans. Ind. Electron.*, vol. 65, no. 3, pp. 2212–2225, Mar. 2018.

[5] H. Groot, E. Janssen, R. Pagano, and K. Schetters, "Design of a 1-MHz LLC resonant converter based on a DSP-driven SOI half-bridge power MOS module," *IEEE Trans. Power Electron.*, vol. 22, no. 6, pp. 2307–2320, Nov. 2007.

[6] E. Orietti, P. Mattavelli, G. Spiazzi, C. Adragna, and G. Gattavari, "Current sharing in three-phase LLC interleaved resonant converter," in *Proc. IEEE Energy Convers. Congr. Expo.*, San Jose, CA, USA, 2009, pp. 1145–1152.

[7] A. K. S. Bhat and R. L. Zheng, "A three-phase series-parallel resonant converter-analysis, design, simulation, and experimental results," *IEEE Trans. Ind. Appl.*, vol. 32, no. 4, pp. 951–960, Jul./Aug. 1996.

[8] A. K. S. Bhat and R. L. Zheng, "Analysis and design of a three-phase LCC-type resonant converter," *IEEE Trans. Aerosp. Electron. Syst.*, vol. 34, no. 3, pp. 508–519, Jul. 1998.

[9] M. S. Almardy and A. K. S. Bhat, "Three-phase (LC)(L)-type series-resonant converter with capacitive output filter," *IEEE Trans. Power Electron.*, vol. 26, no. 4, pp. 1172–1183, Apr. 2011.

[10] Y. Nakakohara, H. Otake, T. M. Evans, T. Yoshida, M. Tsuruya, and K. Nakahara, "Three-phase LLC series resonant DC/DC converter using SiC MOSFETs to realize high-voltage and high-frequency operation," *IEEE Trans. Ind. Electron.*, vol. 63, no. 4, pp. 2103–2110, Apr. 2016.

[11] Y. Tada, M. Uno, and Y. Sato, "Three-phase interleaved LLC asymmetric resonant converter with capacitive current balancing and reduced switch voltage stress," *IEEE Access*, vol. 8, pp. 5688–5698, 2020.

[12] S. A. Arshadi, M. Ordonez, W. Eberle, M. A. Saket, M. Craciun, and C. Botting, "Unbalanced three-phase LLC resonant converters: Analysis and trigonometric current balancing," *IEEE Trans. Power Electron.*, vol. 34, no. 3, pp. 2025–2038, Mar. 2019.

[13] N. Shafiei, M. Ordonez, M. Craciun, C. Botting, and M. Edington, "Burst mode elimination in high-power LLC resonant battery charger for electric vehicles," *IEEE Trans. Power Electron.*, vol. 31, no. 2, pp. 1173–1188, Feb. 2016.

[14] W. Feng, F. C. Lee, and P. Mattavelli, "Optimal trajectory control of burst mode for LLC resonant converter," *IEEE Trans. Power Electron.*, vol. 28, no. 1, pp. 457–466, Jan. 2013.

[15] Q. Cao, Z. Li, and H. Wang, "Wide voltage gain range LLC DC/DC topologies: State-of-the-Art," in *Proc. Int. Power Electron. Conf.*, Niigata, Japan, 2018, pp. 100–107.

[16] N. Shafiei, M. Ordonez, M. A. Saket Tokaldani, and S. A. Arefifar, "PV battery charger using an $L3C$ resonant converter for electric vehicle applications," *IEEE Trans. Transp. Electrific.*, vol. 4, no. 1, pp. 108–121, Mar. 2018.

[17] H. Hu, X. Fang, F. Chen, Z. J. Shen, and I. Batarseh, "A modified high-efficiency LLC converter with two transformers for wide input-voltage range applications," *IEEE Trans. Power Electron.*, vol. 28, no. 4, pp. 1946–1960, Apr. 2013.

[18] W. Sun, Y. Xing, H. Wu, and J. Ding, "Modified high-efficiency LLC converters with two split resonant branches for wide input-voltage range applications," *IEEE Trans. Power Electron.*, vol. 33, no. 9, pp. 7867–7879, Sep. 2018.

[19] C. Kim, J. Baek, and J. Lee, "High-efficiency single-Stage LLC Resonant converter for wide-input-voltage range," *IEEE Trans. Power Electron.*, vol. 33, no. 9, pp. 7832–7840, Sep. 2018.

[20] D. Kim, S. Moon, C. Yeon, and G. Moon, "High efficiency LLC resonant converter with high voltage gain using auxiliary LC resonant circuit," *IEEE Trans. Power Electron.*, vol. 31, no. 10, 2016, pp. 6901–6909, Oct. 2016.

[21] X. Sun, X. Li, Y. Shen, B. Wang, and X. Guo, "Dual-bridge LLC resonant converter with fixed-frequency PWM control for wide input applications," *IEEE Trans. Power Electron.*, vol. 32, no. 1, pp. 69–80, Jan. 2017.

[22] H. Haga and F. Kurokawa, "Modulation method of a full-bridge three-level LLC resonant converter for battery charger of electrical vehicles," *IEEE Trans. Power Electron.*, vol. 32, no. 4, pp. 2498–2507, Apr. 2017.

[23] T. Jiang, J. Zhang, X. Wu, K. Sheng, and Y. Wang, "A bidirectional three-level LLC resonant converter with PWAM control," *IEEE Trans. Power Electron.*, vol. 31, no. 3, pp. 2213–2225, Mar. 2016.

[24] X. Sun, Y. Shen, Y. Zhu, and X. Guo, "Interleaved boost-integrated LLC resonant converter with fixed-frequency PWM control for renewable energy generation applications," *IEEE Trans. Power Electron.*, vol. 30, no. 8, pp. 4312–4326, Aug. 2015.

[25] Y. Jeong, J.-K. Kim, J.-B. Lee, and G.-W. Moon, "An asymmetric half-bridge resonant converter having a reduced conduction loss for DC/DC power applications with a wide range of low input voltage," *IEEE Trans. Power Electron.*, vol. 32, no. 10, pp. 7795–7804, Oct. 2017.

[26] M. I. Shahzad, S. Iqbal, and S. Taib, "Interleaved LLC converter with cascaded voltage-doubler rectifiers for deeply depleted PEV battery charging," *IEEE Trans. Transp. Electrific.*, vol. 4, no. 1, pp. 89–98, Mar. 2018.

[27] H. Wu, X. Zhan, and Y. Xing, "Interleaved LLC resonant converter with hybrid rectifier and variable-frequency plus phase-shift control for wide output voltage range applications," *IEEE Trans. Power Electron.*, vol. 32, no. 6, pp. 4246–4257, Jun. 2017.

[28] G. Liu, Y. Jang, M. M. Jovanović, and J. Q. Zhang, "Implementation of a 3.3-kW DC–DC converter for EV on-board charger employing the series-resonant converter with reduced-frequency-range control," *IEEE Trans. Power Electron.*, vol. 32, no. 6, pp. 4168–4184, Jun. 2017.
[29] H. Wu, Y. Li, and Y. Xing, "LLC resonant converter with semiactive variable-structure rectifier (SA-VSR) for wide output voltage range application," *IEEE Trans. Power Electron.*, vol. 31, no. 5, pp. 3389–3394, May 2016.
[30] M. I. Shahzad, S. Iqbal, and S. Taib, "A wide output range HB-2LLC resonant converter with hybrid rectifier for PEV battery charging," *IEEE Trans. Transp. Electrific.*, vol. 3, no. 2, pp. 520–531, Jun. 2017.
[31] B. Li, F. C. Lee, Q. Li, and Z. Liu, "Bi-directional on-board charger architecture and control for achieving ultra-high efficiency with wide battery voltage range," in *Proc. IEEE Appl. Power Electron. Conf. Expo.*, Tampa, FL, USA, 2017, pp. 3688–3694.
[32] C. Li, H. Wang, and M. Shang, "A five-switch bridge based reconfigurable LLC converter for deeply depleted PEV charging applications," *IEEE Trans. Power Electron.*, vol. 34, no. 5, pp. 4031–4035, May 2019.
[33] H. Wang, M. Shang, and D. Shu, "Design considerations of efficiency enhanced LLC PEV charger using reconfigurable transformer," *IEEE Trans. Veh. Technol.*, vol. 68, no. 9, pp. 8642–8651, Sep. 2019.
[34] S. A. Arshadi, M. Ordonez, M. Mohammadi, and W. Eberle, "Efficiency improvement of three-phase LLC resonant converter using phase shedding," in *Proc. IEEE Energy Convers. Congr. Expo.*, Cincinnati, OH, USA, 2017, pp. 3771–3775.

Sayed Abbas Arshadi (Student Member, IEEE) was born in Isfahan, Iran. He received the B.Sc. degree in electrical engineering from the Malik Ashtar University of Technology, Isfahan, Iran, in 2012, and the M.Sc. degree in electrical engineering (electronics) from the Isfahan University of Technology (IUT), Isfahan, Iran, in 2015. He is currently working toward the Ph.D. degree with the University of British Columbia (UBC), Vancouver, BC, Canada.

From 2013 to 2016, he was a Researcher with the Information and Communication Technology Institute (ICTI), Isfahan, Iran, where he was involved in the design and implementation of power converters. He is also a Research Scholar with Delta-Q Technologies, Burnaby, BC, since 2016. His current research interests include medium and high power dc–dc resonant converters for battery chargers and renewable energy applications.

Martin Ordonez (Member, IEEE) was born in Neuquen, Argentina. He received the Ing. degree in electronics engineering from the National Technological University, Cordoba, Argentina, in 2003, and the M.Eng. and Ph.D. degrees in electrical engineering from the Memorial University of Newfoundland (MUN), St. John's, NL, Canada, in 2006 and 2009, respectively.

He is currently a Professor and Canada Research Chair in power converters for renewable energy systems with the Department of Electrical and Computer Engineering, University of British Columbia, Vancouver, BC, Canada. He is also the holder of the Fred Kaiser Professorship on Power Conversion and Sustainability at UBC. He was an Adjunct Professor with Simon Fraser University, Burnaby, BC, Canada, and MUN. His industrial experience in power conversion includes research and development at Xantrex Technology Inc./Elgar Electronics Corp. (now AMETEK Programmable Power in San Diego, CA, USA). With the support of industrial funds and the Natural Sciences and Engineering Research Council, he has contributed to more than 150 publications and R&D reports.

Dr. Ordonez is a Guest Editor for the IEEE JOURNAL OF EMERGING AND SELECTED TOPICS IN POWER ELECTRONICS, Associate Editor for the IEEE TRANSACTIONS ON POWER ELECTRONICS, and Editor for the IEEE TRANSACTIONS ON SUSTAINABLE ENERGY. He serves on several IEEE committees, and reviews widely for IEEE/IET journals and international conferences. He was the recipient of the David Dunsiger Award for Excellence in the Faculty of Engineering and Applied Science (2009) and the Chancellors Graduate Award/Birks Graduate Medal in 2006, and became a fellow of the School of Graduate Studies, MUN.

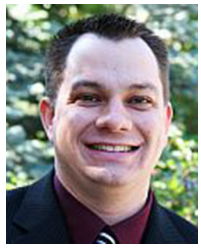

Wilson Eberle (Member, IEEE) received the B.Sc., M.Sc., and Ph.D. degrees from the Department of Electrical and Computer Engineering, Queens University, Kingston, ON, Canada, in 2000, 2003, and 2008, respectively.

He is currently a Tenured Associate Professor with the School of Engineering, University of British Columbia (UBC), Kelowna, BC, Canada. At UBC, he is the Founder and Leader of the Energy Systems and Power Electronics Laboratory. His industrial experience includes positions with Ford Motor Company, Windsor, ON, Canada, and with Astec Advanced Power Systems, Nepean, ON, Canada. He is the author or co-author of more than 90 technical papers published in various IEEE international conferences and IEEE journals. His research interests include high-efficiency power conversion circuits and control techniques for a wide range of industrial and consumer applications.

Dr. Eberle was the recipient of the research grants from the Natural Sciences and Engineering Research Council in Canada, the Canadian Foundation for Innovation, the University of British Columbia, the Kaiser Foundation for Higher Education, and various industry partners.

Marian Craciun (Member, IEEE) received the B.Sc. degree in electronics engineering from the Polytechnic Institute of Bucharest, Bucharest, Romania, in 1989.

He has more than 20 years of experience in developing telecom and industrial power electronics products and sustaining engineering. His industrial experience includes positions with the Energo Repairs RENEL and Asea Brown Boveri Ltd., Bucharest; Argus Technologies Ltd. and Alpha Technologies Ltd., Burnaby, BC, Canada.

He is currently a Senior Power Electronics R&D Engineer with the Delta-Q Technologies Corp., Vancouver, BC, Canada. His current research interests include high-power high-efficiency converter topologies, high-power-factor rectifiers, resonant converters, electric vehicles, and sustainable and renewable energy sources.

Chris Botting (Member, IEEE) received the B.Sc. degree in electrical engineering from Calvin College, Grand Rapids, MI, USA, in 2001.

From 2001 to 2012, he was a Lead Systems Engineer with Azure Dynamics, Burnaby, BC, Canada, a manufacturer of electric and hybrid electric commercial vehicles, with responsibility for energy storage, high-voltage distribution and auxiliary systems, and powertrain architecture. Since 2012, he has been with Delta-Q Technologies, Burnaby, BC, Canada, where he is currently the Manager of Research Engineering, responsible for research activities, funding, university collaboration, intellectual property, and battery test lab functions. His research interests include high-efficiency power converters, electric drive, energy storage, and renewable energy.